Advanced NEMS

Semester Project - Spring 2023

HfC Sputtering parameters optimization and film characterization

Joao Barini Ramos

Supervised by
Pr. Guillermo Villanueva and
Marco Liffredo

Spring 2023

Contents

1 Introduction **3**

2 Theory and methods **3**
- 2.1 Depositions . . . 3
  - 2.1.1 DC Sputtering . . . 3
  - 2.1.2 RF Sputtering . . . 4
  - 2.1.3 RF Bias . . . 4
- 2.2 Film stress measurement . . . 4
- 2.3 Ellipsometry . . . 4
- 2.4 SEM to determine deposition rates . . . 5
- 2.5 Profilometry: Determining deposition rates . . . 5
- 2.6 Resistivity . . . 5

3 Results **5**
- 3.1 Preliminary research . . . 5
- 3.2 RF sputtering . . . 6
  - 3.2.1 Deposition rates . . . 6
  - 3.2.2 Film stress and resistivity . . . 7
- 3.3 DC sputtering . . . 8
  - 3.3.1 Deposition rates . . . 8
  - 3.3.2 Film stress and resistivity . . . 9

4 Ellipsometry **11**

5 Conclusion and future work **13**

A SEM measeurements for thickness determination **15**

B Master Thesis **16**

C Liftoff process for deposition rate determination **17**

D Deposition rates according to recipes **18**

E Deposition performed and wafer flow cards (Excel sheet) **20**

F Ellipsometry results **21**

G Process Flows **30**

H Lab logs **36**

List of Figures

1 Mechanical stress and density of film as a function of ion bombardment [8] . . . 4
2 Compressive stress as a function of resistivity - Thesis . . . 6
3 Deposition rates as a function of sputtering power and different bias powers RF . . . 6
4 Deposition rates expressed as a function of chamber pressure power and different chamber pressures RF . . . 7
5 Film stress as a function of Power and Bias for RF sputtering at constant pressure . 8
6 Film resistivity as a function of Power and Bias for RF sputtering at constant pressure 8
7 Compressive stress vs Resistivity for RF sputtering . . . 8
8 Deposition rates as a function of sputtering power and chamber pressures DC . . . 9

9 Compressive stress as a function of sputtering power in DC at constant pressure . . 10
10 Resistivity as a function of sputtering power in DC at constant pressure 10
11 Stress and resistivity as a function of pressure in DC 11
12 Stress as a function of resistivity for multiple powers and pressures in DC 11
13 Refractive indexes n for RF deposited HfC films 12
14 Extinction coefficients k for RF deposited HfC films 12
15 n and k for DC deposited HfC films 12
16 Cross section of Si wafer deposited using 150W and no bias at 0.005mbar 15
17 Cross section of Si wafer deposited using 200W and no bias at 0.005mbar 15
18 Stress and resistivity as a function of pressure - Thesis 16
19 Stress and resistivity as a function of sputtering power - Thesis 16
20 Liftoff process for deposition rate determination 17
21 Example of thickness measurement using profilometry. 17
22 Recipes developed and deposition rate measurements (RF and DC). 19

Abstract

Hafnium Carbide (HfC) is a refractory ceramic known for its exceptional properties, making it suitable for a wide range of applications. This project investigates the potential utilization of HfC in Micro or Nano Electromechanical Systems (MEMS/NEMS) and explores the effects of physical vapor deposition (PVD) parameters on film stress and resistivity. The study uses RF and DC sputtering with different sputtering powers, pressures and bias power.

Experimental results demonstrate a linear relationship between deposition rates and sputtering power. In RF, compressive stresses increase linearly with sputtering power for bias powers of 0W and 15W, while a minimum stress is observed at a sputtering power of 200W (3.8GPa) with a bias power of 30W. Introducing bias power significantly reduces film stress, with an average reduction of 45% for 30W bias compared to cases without bias. On the other hand, resistivity of the films displays a non-linear dependence on sputtering power. For 30W bias, resistivity initially increases and then decreased with increasing sputtering power.

In DC-sputtered HfC films, while compressive stress decreases with pressure following a power law, resistivity increases exponentially. Resistivity also decreases exponentially with power. Increasing the sputtering power proved to be essential in achieving low resistivity and stress. Notably, the best results are obtained with 300W sputtering power at 0.015 mbar, yielding a low stress of 251 MPa and a resistivity of 0.41 $m\Omega \cdot cm$.

Additionally the optical constants n and k have been determined for RF and DC recipes through ellipsometry. The RF results could resemble to what is found in recent literature, albeit the constants measured for DC present a different behavior, meaning that more trials are needed for certainty.

Acknowledgements

I would like to specially thank Blaise Cuenod, Remi Juttin from the cmi facility, Nicolas Avellan, also working on HfC films, Pr Villanueva and Marco Liffredo for their valuable insights in the project.

1 Introduction

Hafnium Carbide (HfC) is a refractory ceramic exhibiting exceptional properties. With a melting point of about 3900 ºC, it is known to be the binary compound with the highest resistance to melting [3]. This ceramic has high resistance against wear [15], high thermal conductivity and is quite conductive compared to other ceramics [12][9]. Such properties have made HfC suitable for applications in harsh environments in different fields such as in nuclear reactors and in the aerospace industry as heat shields for reentry vehicles [2]. Lately, its high selective absorption coefficients have been exploited for solar panel applications [7]. Despite the remarkable properties, the material has a quite low resistance to oxidation when compared to its high melting point. Past work shows that above 800ºC, HfC starts to oxidize [10] and it is still an active area of research.

To our knowledge, HfC has not yet been used in the fabrication of Micro or Nano Electromechanical Systems (MEMS/NEMS). However, such outstanding properties open a new horizon in terms of potential achievements with the devices. Recent work by F. Bauer [1] amongst other, aimed at attempting micro-machining HfC thin films with IBE and working on a releasing technique compatible with the ceramic. XeF2 and HF have been used leading to unsatisfactory results on the samples provided. A possible reason is due to a high stress on the wafers. Therefore, the present work aims at investigating physical vapour deposition (PVD) parameters on both film stress and conductivity on sputtered HfC films. The goal is to obtain lowest value as possible for those properties. A similar work has been conducted in a master thesis by W. Thongruang [13] in the late 90s using direct current sputtering. His thesis yielded to HfC films with resistivities around 0.3 $m\Omega \cdot cm$ and compressive stresses in the order of 1 GPa for sputtering powers above 350W.

2 Theory and methods

2.1 Depositions

The depositions have been performed using radio frequency (RF) some times with bias and with direct current (DC) generators. The sputtering machine used was the DP 650 by Alliance Concept. During the process, high-energy ions from a plasma collide with a target, causing sputtering and dislodging atoms or molecules. These sputtered species travel through the vacuum, condensing onto the substrate and forming a thin film. Here, sputtering power, bias power and chamber pressure were set at different values. The sputtering power is limited to 300W due to a risk of detachment of the HfC target from the Cu plate holding it in the chamber. Deposition speed, stress and conductivity were measured or calculated for each recipe. The gas flow rate has been kept constant at 30 SCCM and for RF recipes, match box adjusted for each recipe to avoid power reflection.

Deposition rate R_{dep} can be theoretically obtained using Equation 1 [8]. Where γ_{sput} is the sputter yield, Γ_{ion} the ion flux, n_{film} the film density and A correspond to target or substrate area. Ion flux Γ_{ion} is proportional to current, therefore we expect R_{dep} to be proportional to current and to power for a constant voltage.

$$R_{dep} = \frac{\gamma_{sput}\Gamma_{ion}}{n_{film}} \frac{A_{target}}{A_{substrate}} \tag{1}$$

2.1.1 DC Sputtering

In DC sputtering, the target material is negatively charged, and the substrate is held at a grounded or positively charged potential. The positive Ag ions in the plasma are accelerated into the target and the collision causes the ejection of molecules. DC sputtering usually allows a faster deposition rate. However, depending on the material conductivity, charges can build up and result into uneven target consumption and poorer sputtering uniformity.

2.1.2 RF Sputtering

RF sputtering relies on a radio frequency (RF) power supply to generate the plasma. The RF power supply generates a high-frequency alternating current (AC) voltage that is applied to the target electrode thus "cleaning" the charges after every cycle. The RF power supply is also connected to the target electrode through a "match box." It is used to ensure maximum power transfer from the RF power supply. It adjusts the impedance of the RF circuit to minimize reflected power.

2.1.3 RF Bias

RF Bias allows one to control the energy of the ions bombarding the substrate surface. By applying a negative bias voltage to the substrate electrode, the ions are accelerated towards the substrate with a controlled energy. This energy can be adjusted by varying the amplitude of the RF power. Figure 1, presents the relation between film mechanical stress and ion bombardment. RF bias can be used to further enhance the bombardment which for example could lead to either an increase or a decrease in compressive stress (respectively from zone III to IV or from IV to V).

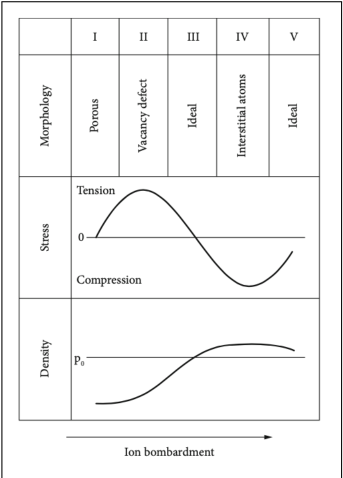

Figure 1: Mechanical stress and density of film as a function of ion bombardment [8]

2.2 Film stress measurement

The film stress has been measured using the FLX 2320-S stress measurement system by Toho Technology. The stress in then computed using Stoney's equation 2 with the difference in the radius of curvature of the wafer due to the film deposition.

$$\sigma = \frac{Eh^2}{(1-\nu)6Rt} \tag{2}$$

where E is the Young's Modulus of the substrate, h the substrate thickness, ν the Poisson ratio, t the film thickness. The substrate radius of curvature R is defined by $1/R = 1/R_2 - 1/R_1$ where R_1 is the leading radius of curvature and R_2 the trailing radius of curvature. The wafers are therefore measured before and after deposition [6].

2.3 Ellipsometry

Despite the lack of optical constants for HfC in the current literature, a first choice for measuring HfC film thickness would be through the use of ellipsometry. This was not possible due to a high absorption in the infrared-visible domain. Nevertheless, once the thicknesses were determined by other means, the optical constants (n,k) for the some recipes have been determined using the Woollam RC2 ellipsometer in the infrared-visible-UV domain for thinner wafers (50nm). The amplitude ratio

and the phase difference have been fitted using a Tauc-Lorentz model similarly to a recent work also for HfC films [5].

2.4 SEM to determine deposition rates

Also with the aim of determining film thickness, the Zeiss LEO 1550 SEM has been used upon cleavage of the wafers and by looking at the cross sections but this method has revealed to be unfeasible for a large quantity of wafers. A lack of precision due to field depth is also to be blamed. Examples of the measurements are presented on Appendix A.

2.5 Profilometry: Determining deposition rates

Each recipe has a different deposition rate that theoretically has to be linear with the sputtering power for a given setup according to Equation 1. Nevertheless, the deposition rates have been determined experimentally by setting a deposition time and by looking at the final thickness with equation 3. Where r is the deposition rate, h the film thickness and t the deposition time.

$$r = \frac{h}{t} \tag{3}$$

Profilometry using the Bruker Dektak XT allowed the film thickness determination upon sputtering. A simple yet effective technique suggested by the Cmi staff consists in using a marker on a Si test wafer and perform a "liftoff" using acetone upon deposition. The thickness of the remaining valleys is then obtained with the profilometer. Considering the large amount of recipes developed for this project, the technique has been adapted so the liftoffs were performed using a wet bench with remover 1165, a stronger solvent, and combined with ultrasound. This has enabled a systematic and faster approach. Appendix C details the process. Considering the linearity of the deposition rates, some few were determined through linear interpolation and such cases are specified.

2.6 Resistivity

The values for resistivity are obtained using the Filmetrics R50-4PP four probes measurement system. First, the square resistance R_s is obtained and resistivity ρ is computed using equation 4 with h being the film thickness. It is important to consider that the comparisons must be made as much as possible with the same film thickness since oxide layers and other effects might alter the final value for resistivity. Resistivity measurements have been conducted exclusively on test Si wafers coated with a 500 nm layer of SiO2 oxide to allow a balanced measurement, excluding the contribution of the Si substrate on the results.

$$\rho = R_s \cdot h \tag{4}$$

3 Results

3.1 Preliminary research

The results concerning film stress and resistivity from Thongruang's thesis [13] are compiled on Figure 2 and Appendix B. Film properties may vary across different machines and wafers even for a same pressure and sputtering power. Therefore those values were solely used to provide an input into the initial parameters to be tested and for comparison purposes. For a given power, compressive stresses decreased and resistivity increased exponentially with pressure. Furthermore, for a given chamber pressure, compressive stresses increased linearly with sputtering power while resistivity decreased exponentially. The lower left corner of Figure 2 is to be aimed. Therefore a high pressure with high sputtering powers are to be privileged to reduce both stress and resistivity.

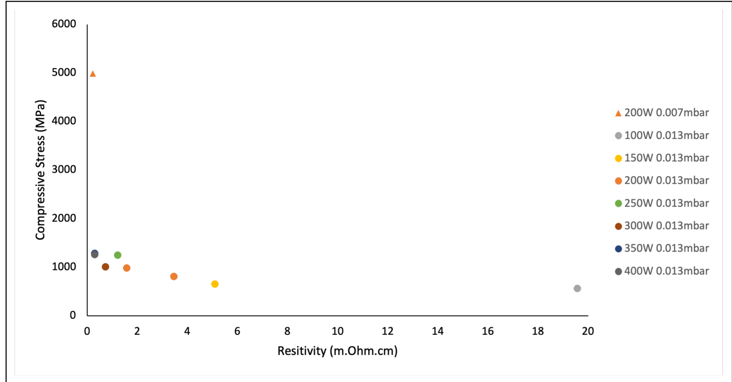

Figure 2: Compressive stress as a function of resistivity from Thongruang's thesis. HfC films were deposited by DC sputtering on Si wafers from pressures varying between 0.0067 mbar and 0.013 mbar and sputtering powers from 100W to 400W.

3.2 RF sputtering

3.2.1 Deposition rates

The first depositions were performed using the RF generator with a chamber pressure of 0.005 mbar, commonly used at the cmi facility. The deposition rates have been measured using the method previously described. Considering the stresses obtained with such recipes (subsubsection 3.2.2), it has become clear that the pressure had to be increased. A pressure of 0.09 mbar has been tried but led to an outlier. Unfortunately it has not been possible to try other recipes under RF due to a technical issue with the generator. Figure 3 and Figure 4 summarize the deposition rates obtained. Detailed values as well as the uniformity measurements are presented in Appendix D. Thanks to Figure 3, we can notice a linear trend with respect to sputtering power across the three biases tested. Furthermore, the deposition rate is reduced with bias power and the slope remains constant across the series of identical bias. While the average deposition rate for 15W and 30W changes by 5%, it is 45% greater for 0W when compared to 30W. For a pressure of 0.005 mbar, the fastest recipe consists in depositing with no bias at 250W. Pressure also has an impact on the deposition rate. Although only two points per series of similar sputtering power, Figure 4 suggests that the depositions speeds clearly reduce with increased pressure. With a higher gas density, this behaviour is likely due to an increased number of atom collisions from the target hindering their path towards the substrate [13].

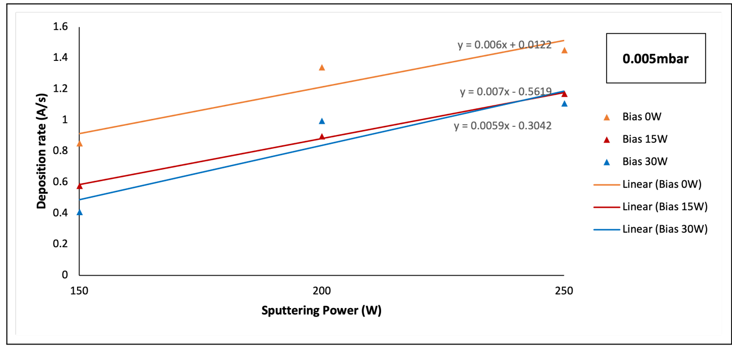

Figure 3: Deposition rates expressed as a function of sputtering power and different bias powers (0W, 15W and 30W). The depositions were made on Si wafers with RF power at a constant pressure of 0.005 mbar. Deposition rates were obtained thanks to a liftoff revealing a valley that was measured with profilometry

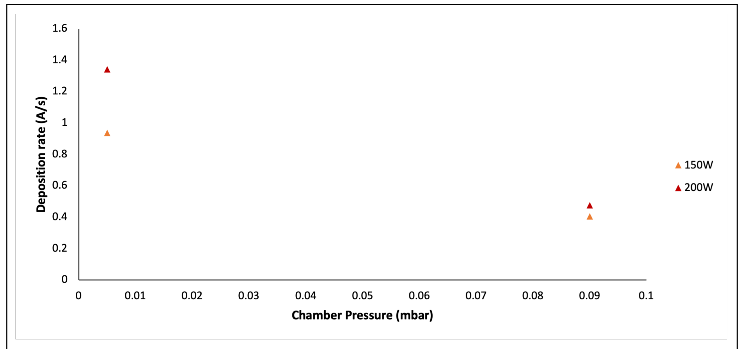

Figure 4: Deposition rates expressed as a function of chamber pressure power and different chamber pressures. The depositions were made on Si wafers with RF power and without bias. Deposition rates were obtained thanks to a liftoff revealing a valley that was measured with profilometry

3.2.2 Film stress and resistivity

Film stresses were calculated for SiO2 wafers and the HfC films have an identical thickness of 50nm to avoid the observation of stress gradient. Deposition machine parameters have been kept constant besides sputtering power and bias. On Figure 5, we can notice that regardless of bias power, the compressive stresses increase linearly with sputtering power for bias of 0W and 15W although with different slopes. However, interestingly when it comes to a bias of 30W, the stresses achieved a minimum for a sputtering power of 200W. In order to further investigate it, two extra depositions have been made for 150W and 200W, confirming this observation.

Bias power allows a significant drop in stress. Indeed in average, the stresses reduce by 45% with the introduction of 30W of bias compared to no bias. This effect tends to be accentuated for increased sputtering power since the slopes are not the same. Physically, one hypothesis explaining this effect is a passage from zone IV into V in Figure 1. On Figure 6, one may notice that an increase in sputtering power does not necessarily imply an increase nor a decrease in resistivity. Notably with a bias of 30W, resistivity increases from 150W to 200W and then decreases for 250W. Furthermore Figure 7 presents an overview of compressive stress plotted against the resistivity. We can observe that resistivity slightly decreases from no bias to 15W and then increases when 30W of bias is used (maybe due to uniformity impact in average thickness).

This is expected and anticipated by theory. Indeed, at lower energies the ion bombardment enhances the packing density of the deposited film, reducing voids and improving interatomic bonding. This increased density leads to a lower resistivity as the charge carriers (electrons) can move more freely through the film. Secondly, it can promote the diffusion of atoms within the film, facilitating the formation of a more uniform and ordered structure. This improved ordering reduces scattering of charge carriers, resulting in lower resistivity. However, as the bias power increases, higher ion energies can cause lattice damage and defect formation within the film such as sputtering gas implantation (Ar) [11]. These defects hinder charge carriers mobility and lead to an increase in resistivity. An x-ray characterization (XRD) could be conducted to study this hypothesis. For comparison purposes, the resistivity range obtained here; 0.25-0.47 $m\Omega cm$, is similar to what can be observed in Titanim Nitride [4] (at ambient temperature), another ceramic.

However, the minimum stress of 3.8 GPa obtained with 200W at 30W of bias remains excessively elevated for micro fabrication purposes. Increasing the chamber pressure might lead to a quick reduction in compressive stress following what is observed for DC sputtering (subsection 3.3). Due to a technical issue with the RF generator, this could not be tried.

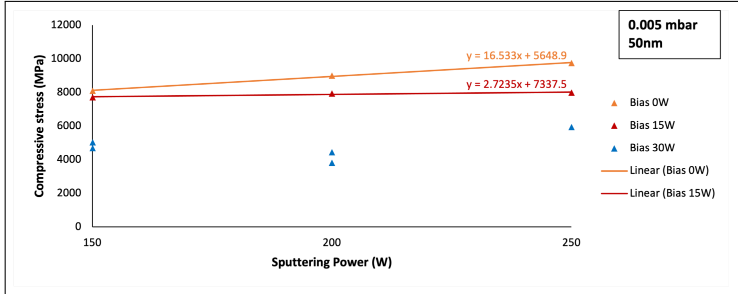

Figure 5: Film stress as a function of Power and Bias for RF sputtering at constant pressure (0.005 mbar)

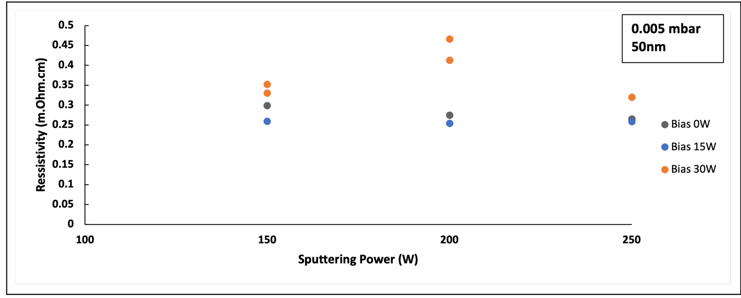

Figure 6: Film resistivity as a function of Power and Bias for RF sputtering at constant pressure (0.005 mbar)

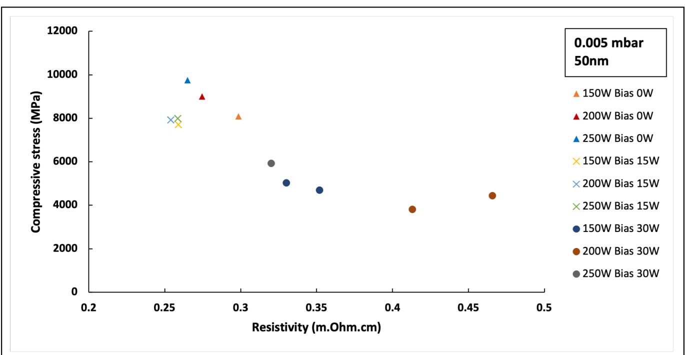

Figure 7: Compressive stress vs resistivity for RF sputtering at constant pressure (0.005 mbar)

3.3 DC sputtering

3.3.1 Deposition rates

Curiously, while in RF the deposition rates reduced with pressure (Figure 4), when using the DC generator Figure 8 reveals the opposite for pressures greater than 0.01 mbar. Most of the data points were obtained using the liftoff method described in subsection 2.5. However, the exceptions are for all the points at 300W and for those at 0.012 and 0.015 mbar respectively, where linear interpolation has been used (linearity assumed). We can notice that this hypothesis holds for recipes with varying powers at the same chamber pressure and is backed-up with equation Equation 1. On the other hand, this is not necessarily the case for recipes with different pressures and same sputtering power. We can also consider that the pressure range is small enough to allow linearity to be assumed. We

note that the fastest recipe in DC corresponds to 300W under a pressure of 0.005 mbar (3Å/s). Furthermore higher deposition rates were obtained with the DC generator as expected. For a same pressure of 0.005 mbar at 200W, a 10% increase has been noted from RF to DC.

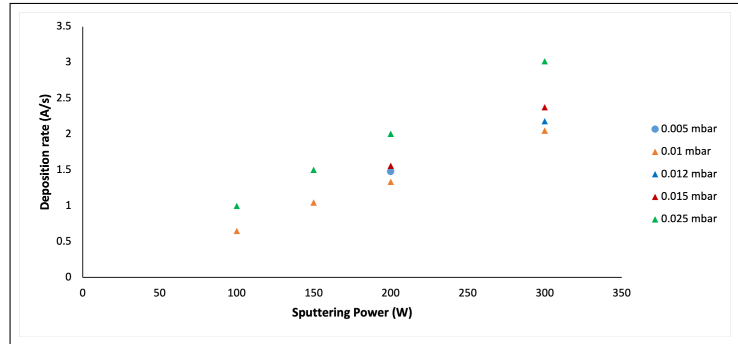

Figure 8: Deposition rates as a function of sputtering power (100W, 150W, 200W and 300W) and varying chamber pressures. The depositions were made on Si wafers with DC power and no bias. Deposition rates were obtained thanks to a liftoff revealing a valley that was measured with profilometry.

3.3.2 Film stress and resistivity

HfC has been deposited on Si wafers coated with a 500nm of SiO2 oxide, similarly to the RF case. In a first moment, thin layers (37nm to 50nm) have been deposited with a constant chamber pressure of 0.025 mbar for sputtering powers between 100W and 200W. A higher pressure has been selected here as a consequence of the results in RF and upon analysis of Thongruang's results [13]. Secondly, the film thickness has been increased to further study the influence of this parameter on stress and resistivity. Finally, 500nm layers of HfC have been deposited also on SiO2 wafers with different pressures at 300W.

Figure 9 reveals that stress tends to remain constant with sputtering power for thinner films. In fact, as the relative standard deviation is at 10%, this variability could be due to randomness. Such observation reveals that an increase in sputtering power has a minor impact on compressive stresses for thinner films. For thicker films, stress increases linearly. On the other hand, it is determinant for resistivity. On Figure 10, we can notice that resistivity decreases exponentially with power (R2=0.99 but 3 points). Therefore, increasing the sputtering power is key in achieving low resistivity and low stress.

Even though, we can notice some stress relaxation with increased thickness for 150W, more data points would be needed in order to establish a conclusion regarding stress gradient. Furthermore, resistivity decreases in average by a 10^4 factor from thin films to thicker. One hypothesis would be due to a larger contribution of an oxide layer on thinner films.

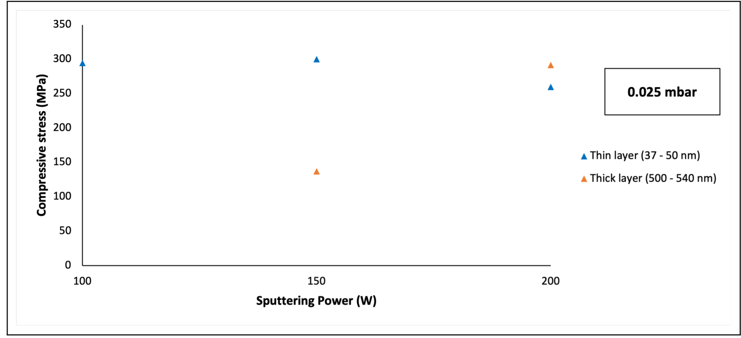

Figure 9: Compressive stress as a function of sputtering power in DC at constant pressure (0.025 mbar)

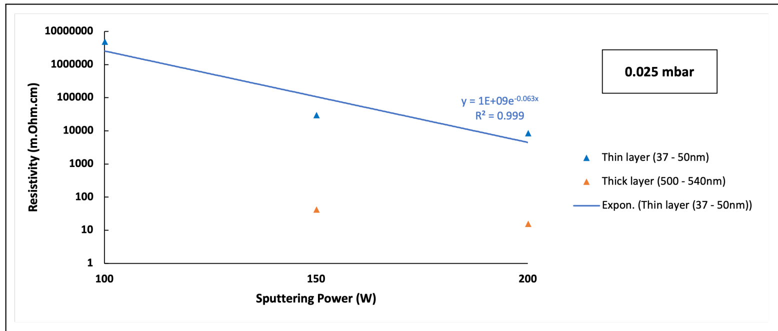

Figure 10: Resistivity as a function of sputtering power in DC at constant pressure (0.025 mbar)

Considering the above results, it has become important to set sputtering power to the maximum allowed (300W) and study how pressure and resistivity relate to chamber pressure. On Figure 11, it is possible to observe that while stress decreases with pressure following a power law, resistivity increases exponentially. Figure 12 confirms that high sputtering powers should be aimed as much as possible to minimize resistivity while one should gradually increase pressure to reduce stress. It is important to closely monitor resistivity as it also increases exponentially with pressure. At the best, with 300W at 0.015 mbar, a low stress of 251 MPa has been obtained with a 0.41 $m\Omega cm$ resistivity. We may note that Thougruang obtained a compressive stress of 1GPa at similar conditions revealing the process and machine dependence on those values.

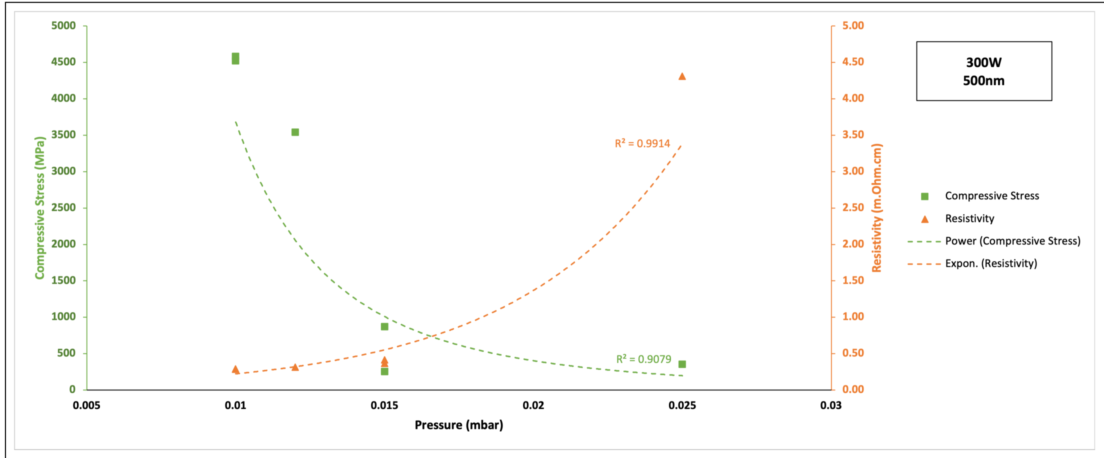

Figure 11: Stress and resistivity as a function of pressure in DC

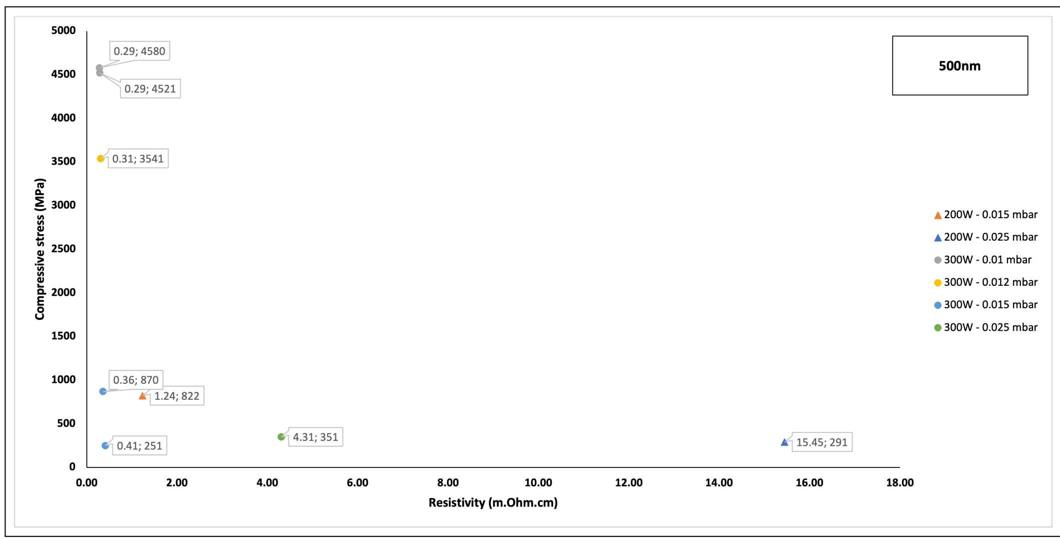

Figure 12: Stress as a function of resistivity for multiple powers and pressures in DC

4 Ellipsometry

Refractive index and extinction coefficients (n and k) for some recipes are detailed on Figure 13, Figure 14 and Figure 15. Amplitude ratio and the phase difference have been modeled using two Tauc-lorentz oscillators and the model's parameters as well as the mean squared errors (MSE) are presented on Appendix F. It is possible to notice that the for wafers deposited with RF, n and k mostly increase with wavelength similarly to what is observed in metals [14] and other absorbing materials. Furthermore, the shape and behaviour of the graphs are comparable to the 2022 study [5]. On the other hand, in the DC case, the optical constants decrease with wave length. Even though with a low MSE, those results should be perhaps retested using a different model.

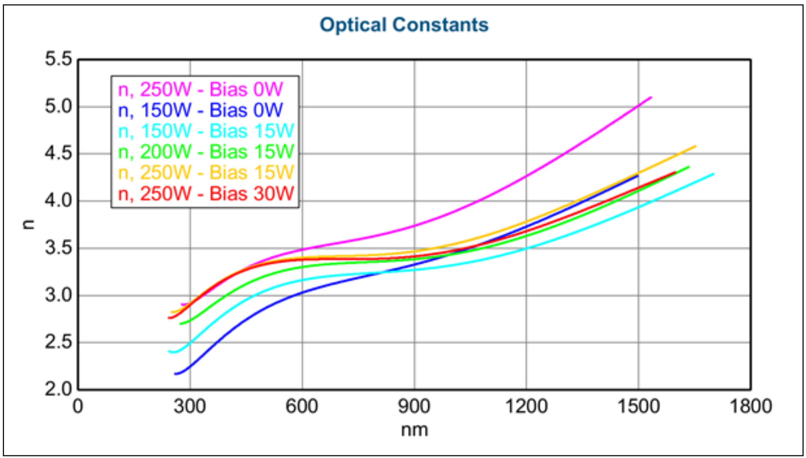

Figure 13: Refractive indexes n for RF deposited HfC films

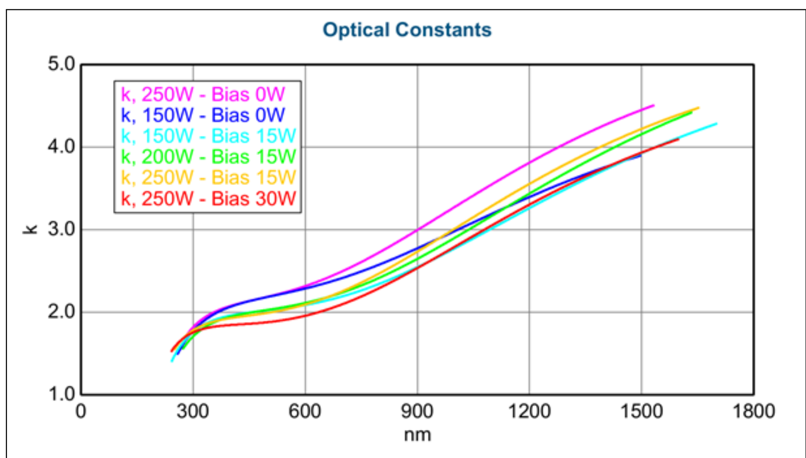

Figure 14: Extinction coefficients k for RF deposited HfC films

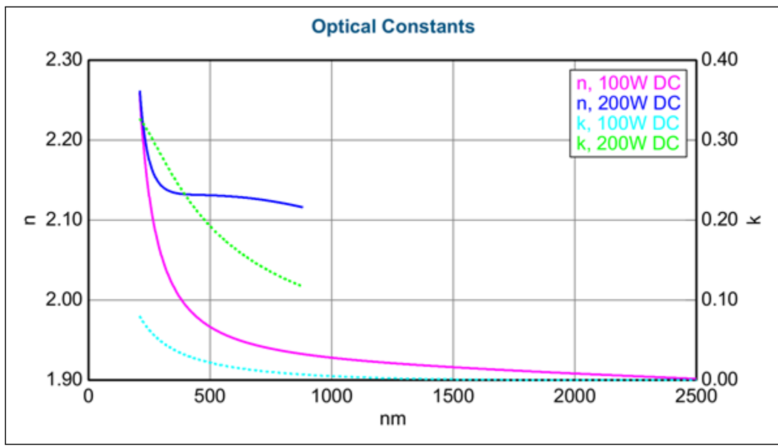

Figure 15: n and k for DC deposited HfC films

5 Conclusion and future work

In summary, the experimental investigation of RF and DC sputtering deposition rates revealed a linear relationship with sputtering power. In the case of DC sputtering, the deposition rates exhibited distinct behavior compared to RF sputtering. Increasing chamber pressure led to an increment in deposition rates for pressures exceeding 0.01 mbar.

Regarding film stress, in RF the results demonstrated that compressive stresses increases linearly with sputtering power for bias powers of 0W and 15W, albeit with varying slopes. However, when a bias power of 30W was employed, the stresses reached a minimum at a sputtering power of 200W (3.8GPa). Introducing bias power notably reduced film stress, with an average reduction of 45% for 30W bias compared to cases without bias. The resistivity of the films does not depend linearly with power. Notably for 30W bias, it increased when using 200W RF. The resistivity dependence on bias power is interesting. In fact, it decreased as bias power increased from 0W to 15W, indicating improved film density and interatomic bonding at lower energies. However, at a bias power of 30W, resistivity increased, likely due to lattice damage and defect formation caused by higher ion energies.

For film stress in DC sputtered HfC films, the results showed relatively constant stress levels with variable sputtering power for thinner films. However, thicker films exhibited a linear increase in stress with sputtering power. Increasing the sputtering power proved to be essential in achieving low resistivity and stress. At the best, with 300W at 0.015 mbar, a low stress of 251 MPa has been obtained with a 0.41 $m\Omega cm$ resistivity. Future work could aim for even higher sputtering powers that were not possible here due to technical limitations.

Additionally optical constants n and k have been determined for RF and DC recipes. While the RF results could resemble to what is found in recent literature, the constants measured for DC present a different behavior meaning that more trials are needed for certainty.

It could be interesting to study the chemical composition of the films using xrd to better understand the crystallographic mechanisms behind stress and resistivity variations. Annealing could also be combined with the recipes to further reduce stress. As an immediate next step, one could try making and releasing HfC MEMS using DC-sputtered films at 300W and 0.025mbar.

References

[1] Fabian Bauer. “Micromachining of Hafnium Carbide”. MA thesis. Lausanne, Switzerland: Ecole Polytechnique Fédérale de Lausanne (EPFL), 2023.

[2] Caroline Brogan. *New record set for world’s most heat resistant material*. URL: https://www.imperial.ac.uk/news/176628/new-record-worlds-most-heat-resistant/. (accessed: 08.06.2023).

[3] Omar Cedillos-Barraza et al. “Investigating the highest melting temperature materials: A laser melting study of the TaC-HfC system”. In: *Scientific Reports* 6 (2016).

[4] Cmi. *DP650 Steps (Pintable version)*. URL: https://www.epfl.ch/research/facilities/cmi/wp-content/uploads/2020/04/DP650_Steps.pdf. (accessed: 19.06.2023).

[5] Daniela De Luca et al. “Detailed studies on sputter-deposited Hf and HfC thin films for solar energy devices”. In: *Solar Energy Materials and Solar Cells* 255 (2023), p. 112304. ISSN: 0927-0248. DOI: https://doi.org/10.1016/j.solmat.2023.112304. URL: https://www.sciencedirect.com/science/article/pii/S0927024823001253.

[6] Quantum Design Europe. *FLX series thin film stress measurement system*. URL: https://qd-europe.com/fileadmin/Mediapool/products/Toho/pdf/FLX_series.pdf. (accessed: 12.06.2023).

[7] Kushagra Hans et al. “Hafnium carbide based solar absorber coatings with high spectral selectivity”. In: *Solar Energy Materials and Solar Cells* 185 (2018), pp. 1–7. ISSN: 0927-0248. DOI: https://doi.org/10.1016/j.solmat.2018.05.005. URL: https://www.sciencedirect.com/science/article/pii/S0927024818302174.

[8] Hamid R. Khan Hartmut Frey. *Handbook of Thin-Film Technology*. Springer, 2015.

[9] E. W. Lindsay and L. J. Berberich. “Electrical Properties of Ceramics as Influenced by Temperature”. In: *Transactions of the American Institute of Electrical Engineers* 67.1 (Jan. 1948), pp. 734–742. ISSN: 2330-9431. DOI: 10.1109/T-AIEE.1948.5059741.

[10] Huan Luo et al. “Mechanical properties, thermal stability and oxidation resistance of HfC/a-C:H films deposited by HiPIMS”. In: *Journal of Alloys and Compounds* 847 (July 2020), p. 156538. DOI: 10.1016/j.jallcom.2020.156538.

[11] Paul Muralt. “Growth of Thin Films”. In: *Class Handout EPFL* (2013).

[12] A. Savvatimskii and S. Onufriev. “Resistivity of Refractory Carbides (ZrC, HfC, and TaC + HfC) in the Solid and Liquid States”. In: *High Temperature* 58 (Nov. 2020), pp. 800–805. DOI: 10.1134/S0018151X20060188.

[13] Wiriya Thongruang. “Synthesis and characterization of Hafnium Carbide thin films”. MA thesis. NJ, USA: New Jersey Institute of Technology, 1997.

[14] Harland Tompkins et al. “Spectroscopic ellipsometry measurements of thin metal films”. In: *Surface and Interface Analysis* 29 (Mar. 2000), pp. 179–187. DOI: 10.1002/(SICI)1096-9918(200003)29:3<179::AID-SIA701>3.0.CO;2-O.

[15] Shuo Wang et al. “Structure, mechanical and tribological properties of HfCx films deposited by reactive magnetron sputtering”. In: *Applied Surface Science* 327 (Jan. 2015). DOI: 10.1016/j.apsusc.2014.11.130.

A SEM measuerements for thickness determination

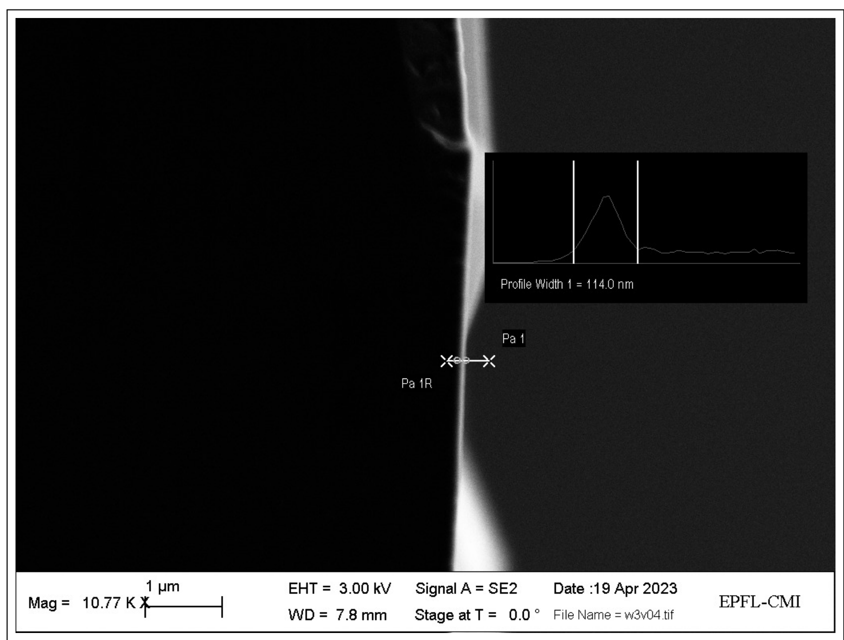

Figure 16: Cross section of Si wafer (center) deposited using 150W and no bias at 0.005mbar. 114nm measured. Expected thickness 168nm (from Appendix D)

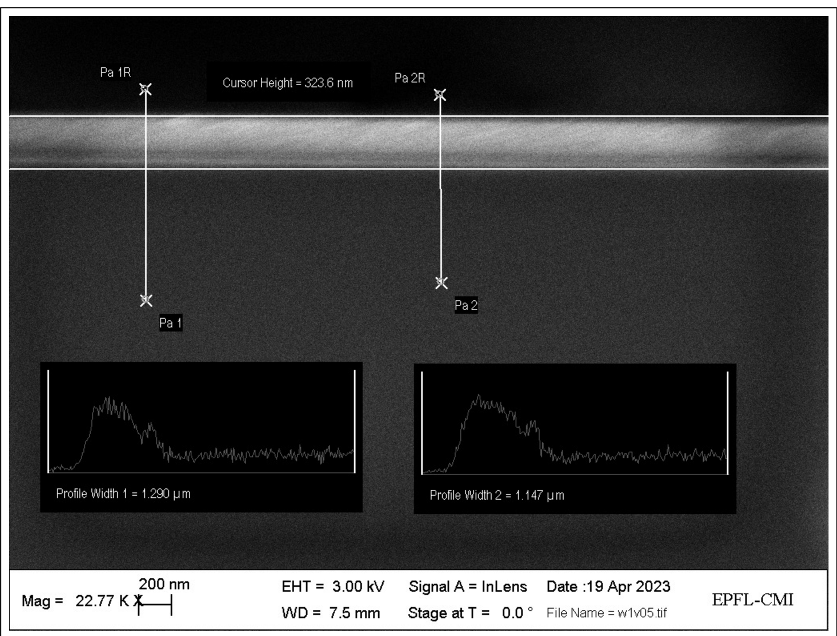

Figure 17: Cross section of Si wafer (center) deposited using RF at 200W and no bias. 324nm measured. Expected thickness 257nm (from Appendix D)

B Master Thesis

Point		Deposition Conditions	
Resistivity (m.Ohm.cm)	Compressive Stress (MPa)	Power (W)	Pressure (mbar)
0.23	4981	200	0.007
3.46	808	200	0.013
19.57	561	100	0.013
5.11	647	150	0.013
1.58	980	200	0.013
1.22	1244	250	0.013
0.73	1007	300	0.013
0.30	1281	350	0.013
0.30	1258	400	0.013

Table 1: Stress and resistivity values obtained from Thongruang's thesis

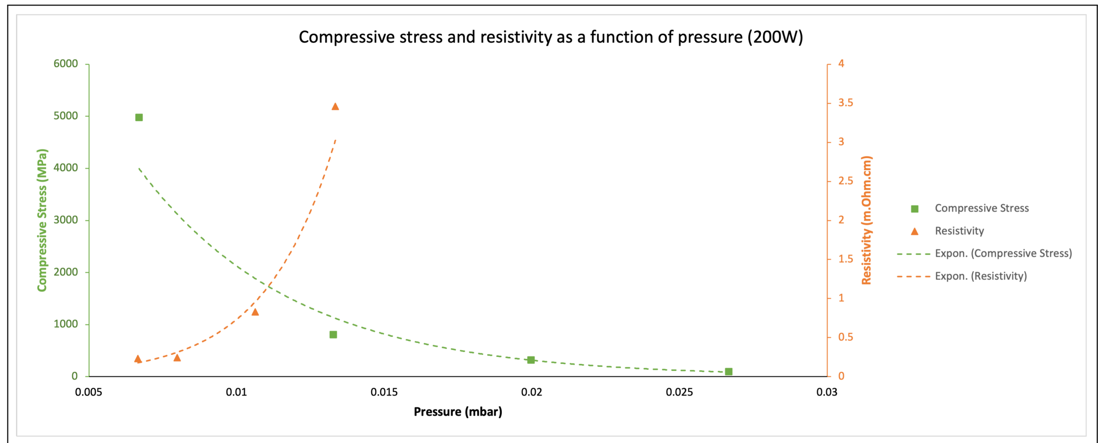

Figure 18: Stress and resistivity as a function of pressure - Thesis

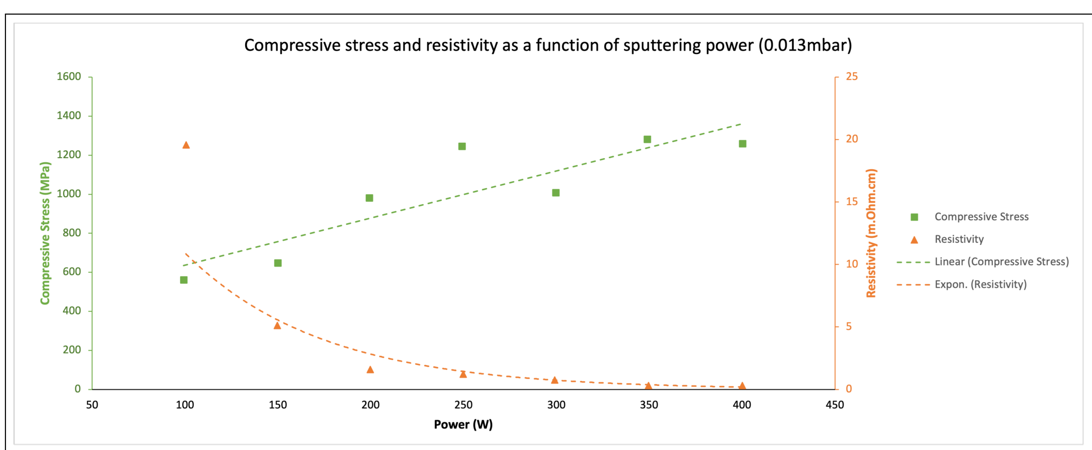

Figure 19: Stress and resistivity as a function of sputtering power - Thesis

C Liftoff process for deposition rate determination

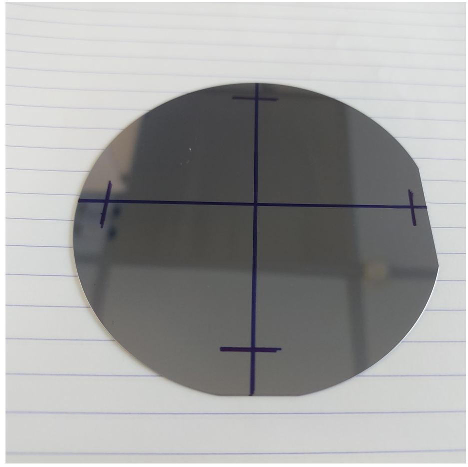

(a) Si test wafer with marker before deposition

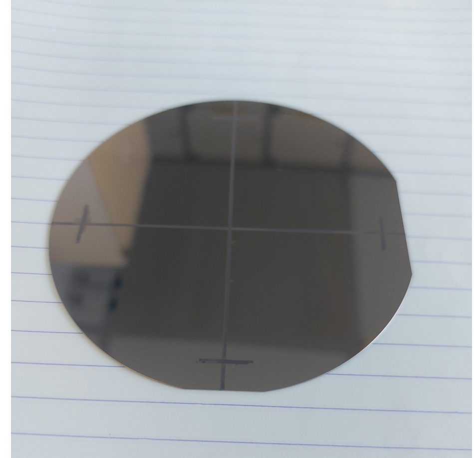

(b) Si test wafer after deposition and before liftoff

Figure 20: Liftoff process for deposition rate determination. Upon deposition, the wafers are inserted in a remover 1165 bath for around 30 min and with ultrasound waves between 5 to 10 min. Then, they are immersed in an isopropanol bath and rinsed twice with water (DI baths) before being dried with N2.

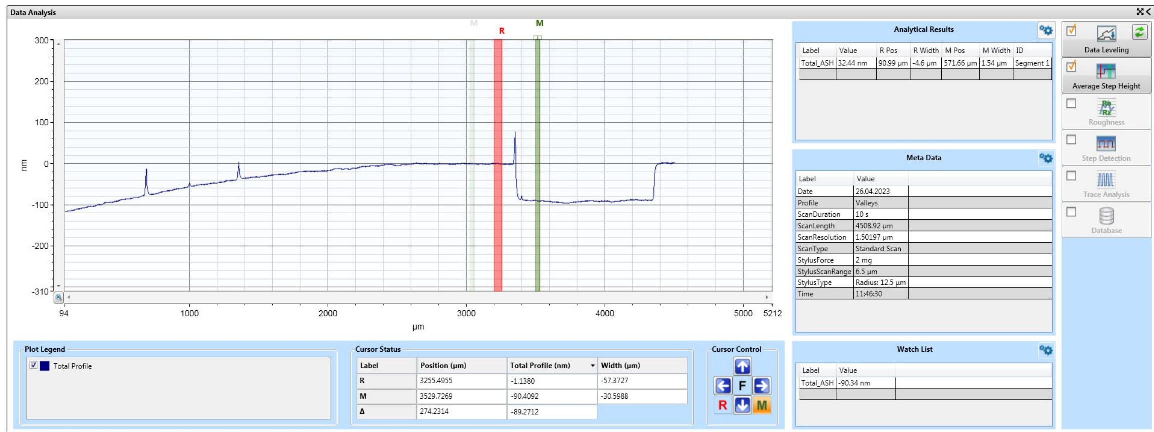

Figure 21: Example of thickness measurement using profilometry.

D Deposition rates according to recipes

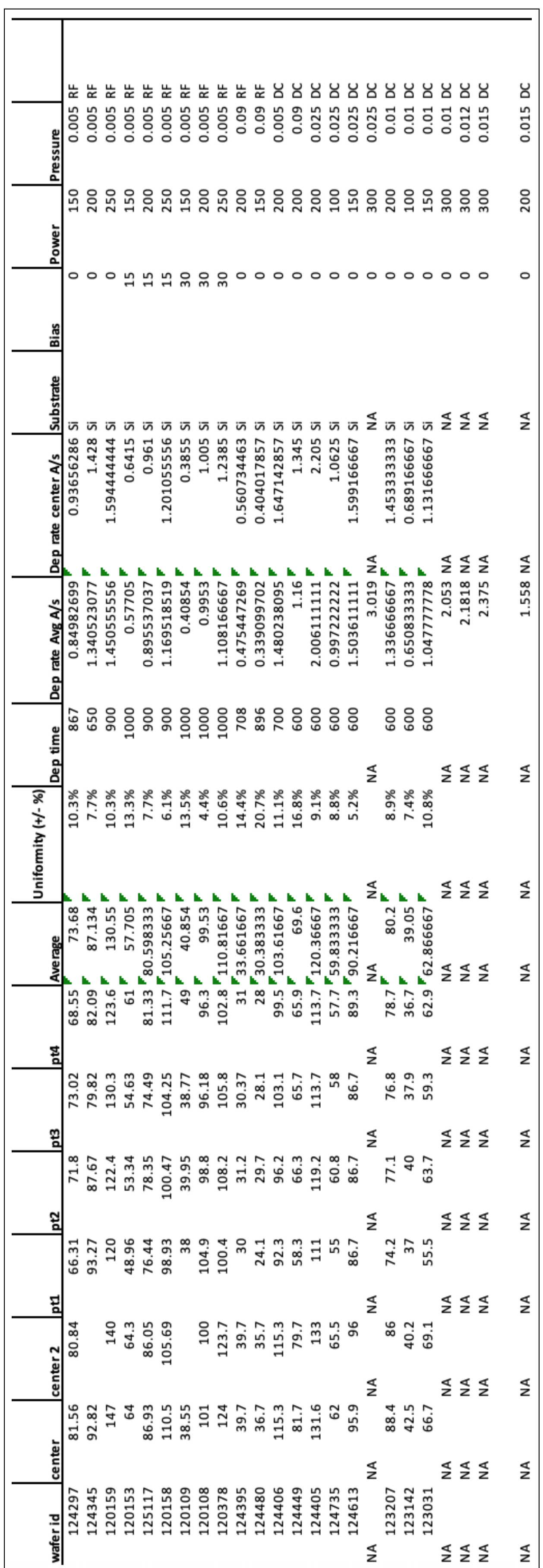

wafer id	center	center 2	pt1	pt2	pt3	pt4	Average	Uniformity (+/- %)	Dep time	Dep rate Avg A/s	Dep rate center A/s	Substrate	Bias	Power	Pressure	
124297	81.56	80.84	66.31	71.8	73.02	68.55	73.68	10.3%	867	0.84982699	0.93656286	Si	0	150	0.005	RF
124345	92.82		93.27	87.67	79.82	82.09	87.134	7.7%	650	1.340523077	1.428	Si	0	200	0.005	RF
120159	147	140	120	122.4	130.3	123.6	130.55	10.3%	900	1.450555556	1.594444444	Si	0	250	0.005	RF
120153	64	64.3	48.96	53.34	54.63	61	57.705	13.3%	1000	0.57705	0.6415	Si	15	150	0.005	RF
125117	86.93	86.05	76.44	78.35	74.49	81.33	80.598333	7.7%	900	0.895537037	0.961	Si	15	200	0.005	RF
120158	110.5	105.69	98.93	100.47	104.25	111.7	105.25667	6.1%	900	1.169518519	1.201055556	Si	15	250	0.005	RF
120109	38.55		38	39.95	38.77	49	40.854	13.5%	1000	0.40854	0.3855	Si	30	150	0.005	RF
120108	101	100	104.9	98.8	96.18	96.3	99.53	4.4%	1000	0.9953	1.005	Si	30	200	0.005	RF
120378	124	123.7	100.4	108.2	105.8	102.8	110.81667	10.6%	1000	1.108166667	1.2385	Si	30	250	0.005	RF
124395	39.7	39.7	30	31.2	30.37	31	33.661667	14.4%	708	0.475447269	0.560734463	Si	0	200	0.09	RF
124480	36.7	35.7	24.1	29.7	28.1	28	30.383333	20.7%	896	0.339099702	0.404017857	Si	0	150	0.09	RF
124406	115.3	115.3	92.3	96.2	103.1	99.5	103.61667	11.1%	700	1.480238095	1.647142857	Si	0	200	0.005	DC
124449	81.7	79.7	58.3	66.3	65.7	65.9	69.6	16.8%	600	1.16	1.345	Si	0	200	0.09	DC
124405	131.6	133	111	119.2	113.7	113.7	120.36667	9.1%	600	2.006111111	2.205	Si	0	200	0.025	DC
124735	62	65.5	55	60.8	58	57.7	59.833333	8.8%	600	0.997222222	1.0625	Si	0	100	0.025	DC
124613	95.9	96	86.7	86.7	86.7	89.3	90.216667	5.2%	600	1.503611111	1.599166667	Si	0	150	0.025	DC
NA	NA	NA	NA	NA	NA	NA	NA	NA	NA	3.019	NA	NA	0	300	0.025	DC
123207	88.4	86	74.2	77.1	76.8	78.7	80.2	8.9%	600	1.336666667	1.453333333	Si	0	200	0.01	DC
123142	42.5	40.2	37	40	37.9	36.7	39.05	7.4%	600	0.650833333	0.689166667	Si	0	100	0.01	DC
123031	66.7	69.1	55.5	63.7	59.3	62.9	62.866667	10.8%	600	1.047777778	1.131666667	Si	0	150	0.01	DC
NA	NA	NA	NA	NA	NA	NA	NA	NA	NA	2.053	NA	NA	0	300	0.01	DC
NA	NA	NA	NA	NA	NA	NA	NA	NA	NA	2.1818	NA	NA	0	300	0.012	DC
NA	NA	NA	NA	NA	NA	NA	NA	NA	NA	2.375	NA	NA	0	300	0.015	DC
NA	NA	NA	NA	NA	NA	NA	NA	NA	NA	1.558	NA	NA	0	200	0.015	DC

Figure 22: Recipes developed and deposition rate measurements (RF and DC). Uniformity using: (MAX - MIN)/(2*AVERAGE)*100%. NA indicates the use of linear interpolation.

E Deposition performed and wafer flow cards (Excel sheet)

Contact Nicolas Avellan or Joao Barini for shareable link.

F Ellipsometry results

Sample: 121717 - RF 250W Bias 0W 0.005mbar

Fit Results	Optical Model
MSE = 4.703 Roughness = 8.21 ± 0.068 nm Thickness # 2 = 51.23 ± 0.087 nm Einf = 0.703 ± 0.5034 UV Pole Amp. = 140.0964 ± 27.16218 UV Pole En. = 6.362 ± 0.1993 Amp1 = 83.2278 ± 1.77280 Br1 = 12.476 ± 9999.0000 Eo1 = 4.471 ± 0.0630 Eg1 = 0.00 ± 0.0481 Amp2 = 73.8413 ± 6.01678 Br2 = 34.504 ± 9999.0000 Eo2 = 0.554 ± 0.0248 Eg2 = 0.00 ± 0.0217 % Thickness Non-uniformity = 0.00 ± 2.147	Roughness = **8.21 nm** (fit) + Layer # 2 = Gen-Osc Thickness # 2 = **51.23 nm** (fit) Layer # 1 = SiO2_JAW Thickness # 1 = 500.00 nm Substrate = Si_JAW3

Experimental and Model Generated Data Fits

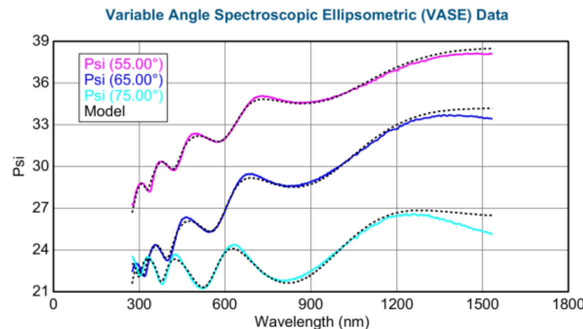

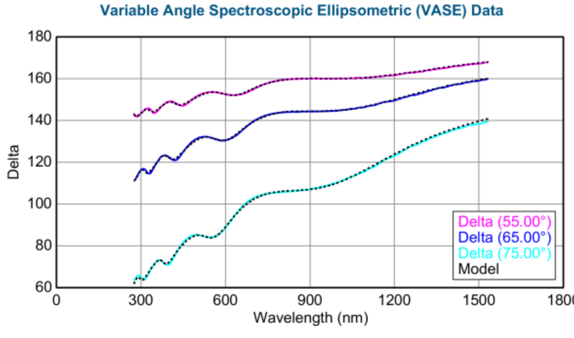

Sample: 121805 - RF 150W Bias 0W 0.005mbar

<table>
<tr>
<td>

Fit Results

MSE = 12.992
Roughness = 2.06 ± 0.383 nm
Einf = 0.00 ± 1.2788
UV Pole Amp. = 138.6418 ± 83.50859
UV Pole En. = 7.024 ± 0.6772
IR Pole Amp. = 3.6605 ± 3.69748
Amp1 = 65.6628 ± 6.86850
Br1 = 12.476 ± 4.3491E-10
Eo1 = 3.716 ± 0.1722
Eg1 = 0.0985 ± 0.1683
Amp2 = 66.1496 ± 95.73598
Br2 = 34.504 ± 9999.0000
Eo2 = 0.530 ± 0.3415
Eg2 = 0.0680 ± 0.3575
Thickness # 1 = 502.28 ± 2.018 nm
% Thickness Non-uniformity = 0.00 ± 4.904

</td>
<td>

Optical Model

Roughness = **2.06 nm** (fit)
+ Layer # 2 = Gen-Osc Thickness # 2 = 55.00 nm
Layer # 1 = SiO2_JAW Thickness # 1 = **502.28 nm** (fit)
Substrate = Si_JAW3

</td>
</tr>
</table>

Experimental and Model Generated Data Fits

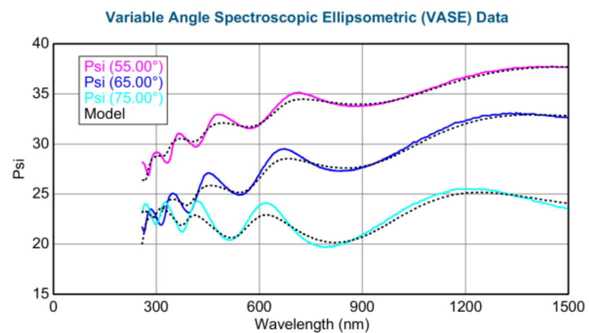

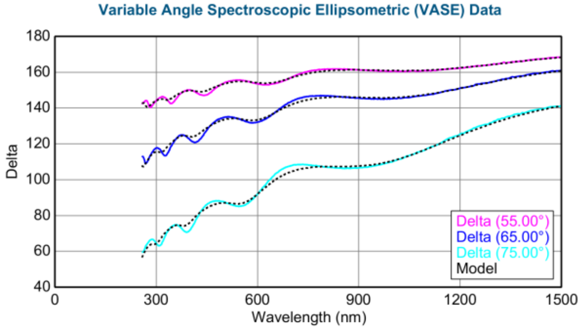

Sample: 120921 - RF 250W Bias 15W 0.005mbar

Fit Results	Optical Model
MSE = 10.621 Roughness = 4.17 ± 0.080 nm Einf = 0.0455 ± 0.8011 UV Pole Amp. = 160.8032 ± 54.73818 UV Pole En. = 7.223 ± 0.3902 IR Pole Amp. = 3.6419 ± 2.50657 Amp1 = 69.7235 ± 2.03793 Br1 = 12.476 ± 2.8804E-10 Eo1 = 4.214 ± 0.0772 Eg1 = 0.00 ± 0.0573 Amp2 = 62.2082 ± 65.76675 Br2 = 34.504 ± 9999.0000 Eo2 = 0.465 ± 0.2077 Eg2 = 0.0400 ± 0.2364 % Thickness Non-uniformity = 0.00 ± 3.285	Roughness = 4.17 nm (fit) + Layer # 2 = Gen-Osc Thickness # 2 = 56.00 nm Layer # 1 = SiO2_JAW Thickness # 1 = 500.00 nm Substrate = Si_JAW3

Experimental and Model Generated Data Fits

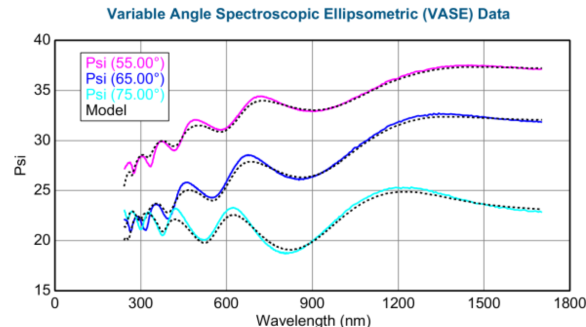

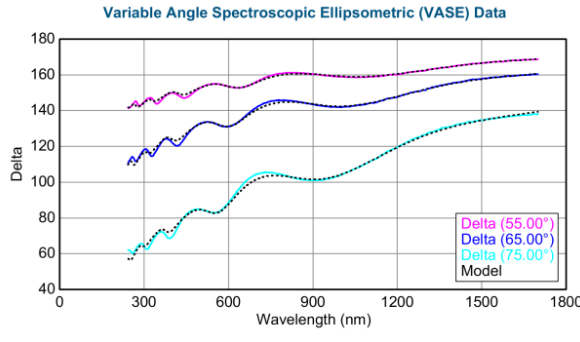

Sample: 120557 - RF 200W Bias 15W 0.005mbar

Fit Results	Optical Model
MSE = 4.806 Roughness = 6.29 ± 0.034 nm Einf = 0.212 ± 0.7115 UV Pole Amp. = 176.9445 ± 46.29388 UV Pole En. = 6.863 ± 0.3038 IR Pole Amp. = 3.8150 ± 1.76786 Amp1 = 73.9410 ± 1.13019 Br1 = 12.476 ± 1.5246E-10 Eo1 = 4.282 ± 0.0492 Eg1 = 0.00 ± 0.0323 Amp2 = 66.1407 ± 41.87966 Br2 = 34.504 ± 9999.0000 Eo2 = 0.476 ± 0.1251 Eg2 = 0.0275 ± 0.1486 % Thickness Non-uniformity = 0.00 ± 1.687	Roughness = **6.29 nm** (fit) + Layer # 2 = Gen-Osc Thickness # 2 = 53.60 nm Layer # 1 = SiO2_JAW Thickness # 1 = 500.00 nm Substrate = Si_JAW3

Experimental and Model Generated Data Fits

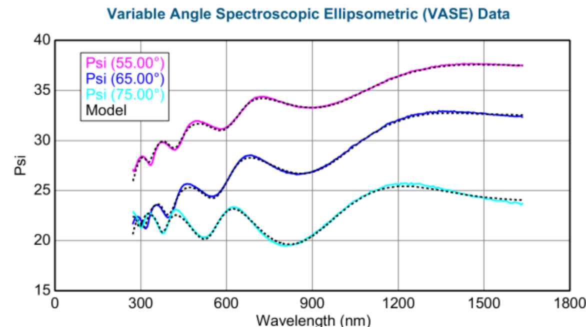

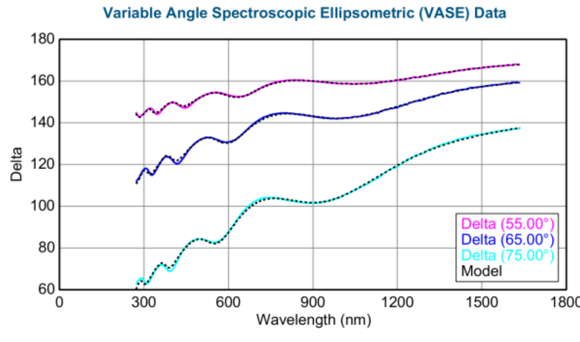

Sample: 120858 - RF 250W Bias 15W 0.005mbar

Fit Results	Optical Model
MSE = 4.479 Roughness = 7.64 ± 0.029 nm Einf = 0.719 ± 0.5595 UV Pole Amp. = 185.2516 ± 40.57837 UV Pole En. = 7.276 ± 0.2638 IR Pole Amp. = 5.9114 ± 0.93253 Amp1 = 83.7385 ± 1.18986 Br1 = 12.476 ± 9999.0000 Eo1 = 4.862 ± 0.0557 Eg1 = 0.00 ± 0.0360 Amp2 = 67.0532 ± 19.88541 Br2 = 34.504 ± 9999.0000 Eo2 = 0.541 ± 0.0697 Eg2 = 0.0408 ± 0.0782 % Thickness Non-uniformity = 2.25 ± 0.407	Roughness = **7.64 nm** (fit) + Layer # 2 = Gen-Osc Thickness # 2 = 51.30 nm Layer # 1 = SiO2_JAW Thickness # 1 = 500.00 nm Substrate = Si_JAW3

Experimental and Model Generated Data Fits

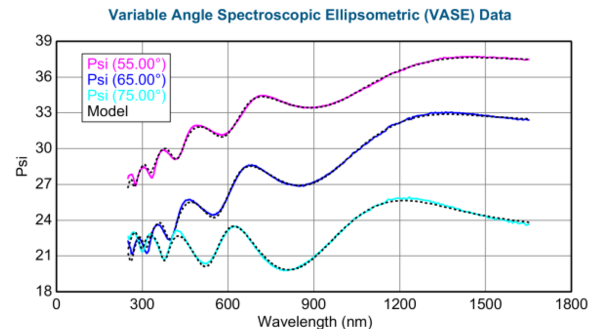

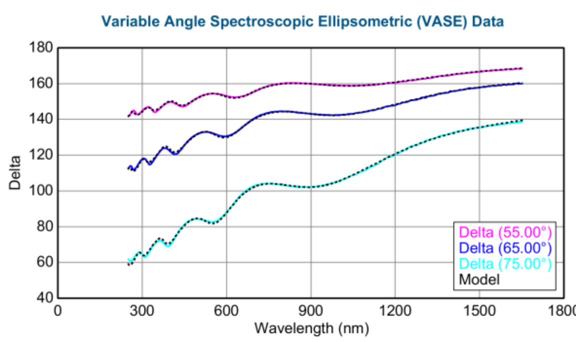

Sample: 120874 - RF 250W Bias 30W 0.005mbar

Fit Results	Optical Model
MSE = 4.825 Thickness # 2 = 45.28 ± 0.027 nm Einf = 1.654 ± 0.4006 UV Pole Amp. = 117.2358 ± 25.89460 UV Pole En. = 7.059 ± 0.2402 IR Pole Amp. = 5.6593 ± 0.89917 Amp1 = 83.7898 ± 0.99837 Br1 = 12.476 ± 4.4851E-10 Eo1 = 5.099 ± 0.0583 Eg1 = 0.00 ± 0.0341 Amp2 = 57.5873 ± 17.91457 Br2 = 34.504 ± 9999.0000 Eo2 = 0.556 ± 0.0745 Eg2 = 0.0333 ± 0.0856 % Thickness Non-uniformity = 0.44 ± 0.602	Roughness = 7.67 nm + Layer # 2 = Gen-Osc Thickness # 2 = **45.28 nm** (fit) Layer # 1 = SiO2_JAW Thickness # 1 = 500.00 nm Substrate = Si_JAW3

Experimental and Model Generated Data Fits

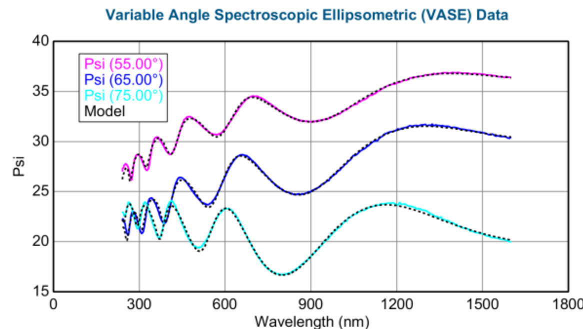

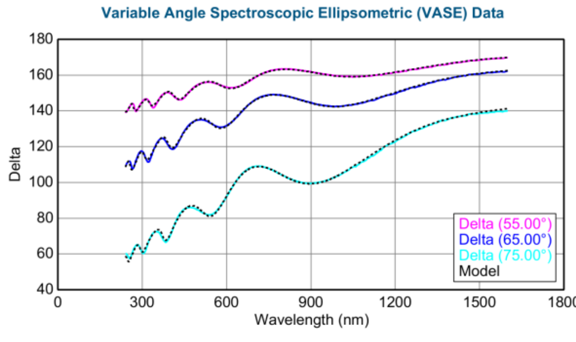

Sample: 120841 – DC 100W 0.025mbar

<table>
<tr>
<td>

Fit Results
MSE = 19.962
Roughness = 5.92 ± 0.089 nm
Thickness # 2 = 53.34 ± 0.047 nm
Einf = 1.028 ± 33.7589
UV Pole Amp. = 0.8829 ± 17406.09749
UV Pole En. = 15.000 ± 104432.6132 (Error-Exceeds-Limit)
IR Pole Amp. = 0.0127 ± 0.00408
Amp1 = 16.9452 ± 207.92112
Br1 = 0.0632 ± 1.9471
Eo1 = 8.921 ± 8.6568
Eg1 = 0.673 ± 48.5791
Amp2 = 18.0500 ± 779.58183
Br2 = 10.541 ± 184.9016
Eo2 = 15.000 ± 123.5731
Eg2 = 0.606 ± 1.1320
% Thickness Non-uniformity = 0.60 ± 0.0437

</td>
<td>

Optical Model
Roughness = 5.92 nm (fit)
+ Layer # 2 = Gen-Osc Thickness # 2 = 53.34 nm (fit)
Layer # 1 = SiO2_JAW Thickness # 1 = 511.38 nm
Substrate = Si_JAW3

</td>
</tr>
</table>

Experimental and Model Generated Data Fits

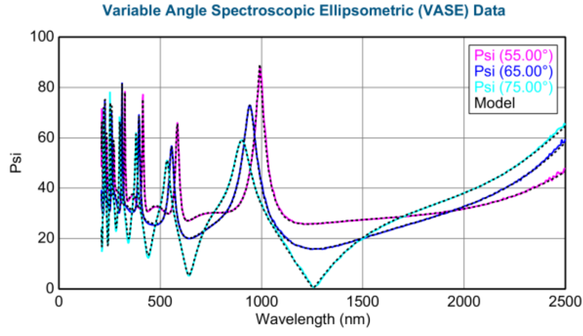

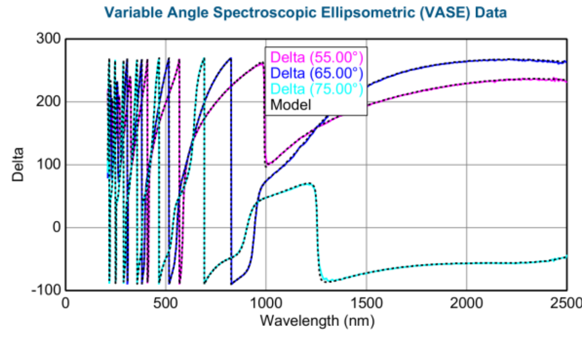

Sample: 123180 – DC 200W 0.025mbar

<table>
<tr>
<td>

Fit Results
MSE = 28.425
Roughness = 4.69 ± 0.114 nm
Thickness # 2 = 57.11 ± 0.148 nm
Einf = 0.782 ± 1.2625
UV Pole Amp. = 21.0729 ± 917.54558
UV Pole En. = 8.036 ± 12.6820
IR Pole Amp. = 0.3085 ± 0.09382
Amp1 = 24.3443 ± 169.31171
Br1 = 0.720 ± 13.7363
Eo1 = 9.181 ± 13.6947
Eg1 = 2.148 ± 1.6993
Amp2 = 23.3361 ± 36.57824
Br2 = 35.409 ± 1.2968E-09
Eo2 = 11.344 ± 10.5287
Eg2 = 0.00 ± 0.1803
Thickness # 1 = 512.21 ± 0.192 nm
% Thickness Non-uniformity = 0.73 ± 0.102

</td>
<td>

Optical Model
Roughness = 4.69 nm (fit)
+ Layer # 2 = Gen-Osc Thickness # 2 = 57.11 nm (fit)
Layer # 1 = SiO2_JAW Thickness # 1 = 512.21 nm (fit)
Substrate = Si_JAW3

</td>
</tr>
</table>

Experimental and Model Generated Data Fits

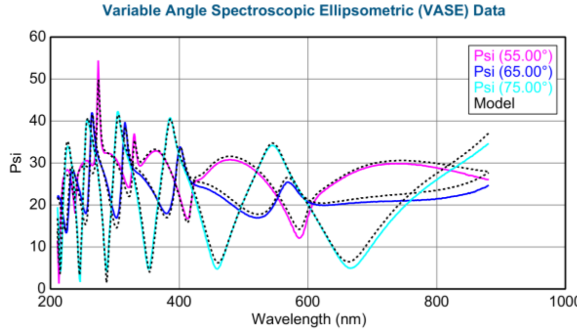

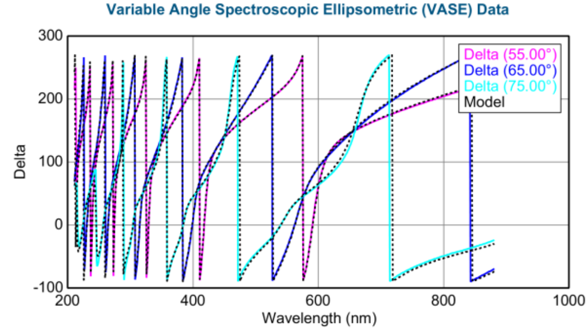

G Process Flows

Lab : Advanced NEMS
Operator Name : **Nicolas Avellan, Joao Barini**
Supervisor Name : Guillermo Villanueva

Phone : 0798695887
Office :
E-mail : nicolas.avellanmarin@epfl.ch
joao.bariniramos@epfl.ch

☒ Semestral Project ☐ Master Project ☐ Thesis ☐ Other

Project Name: Characterisation of HfC thin films deposition

Description of the fabrication project

The goal is to optimize the deposition and annealing techniques of Hafnium Carbide. We aim at creating a deposition protocol for multiple thicknesses as well as an annealing protocol to reduce the observed brittlness of HfC. We analyse and improve electrical conductivity of the samples to complete the analysis.

Technologies used *!! remove non-used !!*
Sputtering, Annealing, Ellipsometry, Optical metrology

Ebeam litho data - Photolitho masks - Laser direct write data			
Mask #	**Critical Dimension**	**Critical Alignment**	**Remarks**

Substrate Type
Silicon wafer + Oxide (100mm <100>, 525 um thickness, 500nm SiO2 Oxide), HfC layer (200-2000um)

Interconnections and packaging of final device

Thinning/grinding/polishing of the samples is required at some stage of the process.

☒ No ☐ Yes => confirm involved materials with CMi staff

Dicing of the samples is required at some stage of the process.

☒ No ☐ Yes => confirm dicing layout with CMi staff

Wire-bonding of dies, with glob-top protection, is required at the end of the process.

☒ No ☐ Yes => confirm pads design (size, pitch) and involved materials with CMi staff

Lab : Advanced NEMS
Operator Name : **Nicolas Avellan, Joao Barini**
Supervisor Name : Guillermo Villanueva

Phone : 0798695887
Office :
E-mail : nicolas.avellanmarin@epfl.ch
joao.bariniramos@epfl.ch

Step-by-step process outline

Step	Process description	Cross-section after process
1.	***Wafer stress measurement*** Tool: Z15 Toho FLX	Silicon + oxide substrate
2.	***HfC deposition*** Tool: Z11 Alliance-Concept DP650 Thickness : 100nm – 1um (to evaluate with CMi staff)	HfC Silicon + oxide substrate
3.	*Optical measurement* Tool: Z4 Woodlam RC2	HfC Silicon + oxide substrate
4.	*Film Stress Measurement* Machine: Z15 Toho FLX	HfC Silicon + oxide substrate
5.	*Sheet resistance Measurement* Machine: Z4 Filmetrics R50	HfC Silicon + oxide substrate
6.	*Annealing* Machine: Z11 Neytech Qex Slope : 20K/min T_max : 600°C Time spent at T_max : 15min Atmosphere : Nitrogen	HfC Silicon + oxide substrate
7.	*Plane Stress Measurement* Machine: Z15 Toho Technology FLX	HfC Silicon substrate
8.	*Optical measurement* Tool: Z4 Woodlam RC2	HfC Silicon + oxide substrate
9.	*Sheet resistance Measurement* Machine: Z4 Filmetrics R50	HfC Silicon + oxide substrate

Lab : Advanced NEMS
Operator Name : Joao Barini Ramos, Nicolas Avellin
Supervisor Name : Guillermo Villanueva

Phone : +33672385437
Office :
E-mail : joao.bariniramos@epfl.ch nicolas.avellanmarin@epfl.ch

CMi EPFL Center of MicroNanoTechnology

☒ Semestral Project ☐ Master Project ☐ Thesis ☐ Other

Project Name: Characterisation of HfC thin films deposition

Description of the fabrication project

The goal is to measure residual plane stress of an HfC layer (200-2000 nm) before and after it has been annealed.
Interest parameters : residual stress, annealing time, annealing temperature preset (CHECK)
Also need to determine deposition rates of the different recipes for the deposition.

Technologies used *!! remove non-used !!*			
Sputtering, Annealing, Ellipsometry, Optical metrology			
Ebeam litho data - Photolitho masks - Laser direct write data			
Mask #	**Critical Dimension**	**Critical Alignment**	**Remarks**
Substrate Type			
Silicon wafer (100mm <100>, 525 um thickness), HfC layer (200-2000um)			

Interconnections and packaging of final device

Thinning/grinding/polishing of the samples is required at some stage of the process.
☒ No ☐ Yes => confirm involved materials with CMi staff

Dicing of the samples is required at some stage of the process.
☒ No ☐ Yes => confirm dicing layout with CMi staff

Wire-bonding of dies, with glob-top protection, is required at the end of the process.
☒ No ☐ Yes => confirm pads design (size, pitch) and involved materials with CMi staff

Phone : +33672385437
Office :
E-mail : joao.bariniramos@epfl.ch nicolas.avellanmarin@epfl.ch

Step-by-step process outline

Step	Process description	Cross-section after process
1.	***Wafer stress measurement*** Tool: Z15 Toho FLX	Silicon substrate
2.	***Marker drawing*** *Using marker*	Silicon substrate
3.	***HfC deposition*** Tool: Z11 Alliance-Concept DP650 Thickness : 100nm – 1um (to evaluate with CMi staff)	HfC Silicon substrate
4.	*Film Stress Measurement* Machine: Z15 Toho FLX	HfC Silicon substrate
5.	*LiftOff* *Machine: wet bench* *Solvent: Acetone*	HfC Silicon substrate
6.	*Profilometry for thickness measurement* *Machine:* Z4 Bruker Dektak XT	HfC Silicon substrate
7.	*Sheet resistance Measurement* Machine: Z4 Filmetrics R50	HfC Silicon substrate
8.	*Annealing* Machine: Z11 Neytech Qex	HfC Silicon substrate
9.	*Plane Stress Measurement* Machine: Z15 Toho Technology FLX	HfC Silicon substrate

10.	*Optical measurement* Tool: Z4 Woodlam RC2	HfC Silicon substrate
11.	*Sheet resistance Measurement* Machine: Z4 Filmetrics R50	HfC Silicon substrate

H Lab logs